Mycobacteria release active membrane vesicles that modulate immune responses in a TLR2-dependent manner in mice

Rafael Prados-Rosales,[1] Andres Baena,[1] Luis R. Martinez,[2] Jose Luque-Garcia,[3] Rainer Kalscheuer,[4] Usha Veeraraghavan,[5] Carmen Camara,[3] Joshua D. Nosanchuk,[1,2] Gurdyal S. Besra,[5] Bing Chen,[1,6] Juan Jimenez,[7] Aharona Glatman-Freedman,[8] William R. Jacobs Jr.,[1,6,9] Steven A. Porcelli,[1,2] and Arturo Casadevall[1,2]

[1]Department of Microbiology and Immunology, and [2]Department of Medicine, Albert Einstein College of Medicine, New York, New York, USA. [3]Department of Analytical Chemistry, Universidad Complutense de Madrid, Madrid, Spain. [4]Institute for Medical Microbiology and Hospital Hygiene, Heinrich-Heine-University Düsseldorf, Düsseldorf, Germany. [5]School of Chemistry, University of Birmingham, Edgbaston, Birmingham, United Kingdom. [6]Department of Genetics, [7]Analytical Imaging Facility, Department of Anatomy and Structural Biology, [8]Department of Pediatrics, and [9]Howard Hughes Medical Institute, Albert Einstein College of Medicine, New York, New York, USA.

Bacteria naturally release membrane vesicles (MVs) under a variety of growth environments. Their production is associated with virulence due to their capacity to concentrate toxins and immunomodulatory molecules. In this report, we show that the 2 medically important species of mycobacteria, *Mycobacterium tuberculosis* and *Mycobacterium bovis* bacille Calmette-Guérin, release MVs when growing in both liquid culture and within murine phagocytic cells in vitro and in vivo. We documented MV production in a variety of virulent and nonvirulent mycobacterial species, indicating that release of MVs is a property conserved among mycobacterial species. Extensive proteomic analysis revealed that only MVs from the virulent strains contained TLR2 lipoprotein agonists. The interaction of MVs with macrophages isolated from mice stimulated the release of cytokines and chemokines in a TLR2-dependent fashion, and infusion of MVs into mouse lungs elicited a florid inflammatory response in WT but not TLR2-deficient mice. When MVs were administered to mice before *M. tuberculosis* pulmonary infection, an accelerated local inflammatory response with increased bacterial replication was seen in the lungs and spleens. Our results provide strong evidence that actively released mycobacterial vesicles are a delivery mechanism for immunologically active molecules that contribute to mycobacterial virulence. These findings may open up new horizons for understanding the pathogenesis of tuberculosis and developing vaccines.

Introduction

Many intracellular bacterial pathogens use membrane vesicles (MVs) as an alternative way to deliver ligands that can be recognized by host cells (1, 2). These MVs have been extensively studied in Gram-negative bacteria, which release MVs into the surrounding environment by a process that involves budding and "pinching off" from the outer membrane (3). The vesicles vary in size from 50 to 250 nm in diameter and contain phospholipids, proteins, and LPS as well as periplasmic components (3). Certain MVs can carry additional virulence factors, such as toxins, adhesins, or immunomodulatory compounds that are important for pathogenesis (1). Recently, a vesicular transport system has been described in the Gram-positive bacterium *Bacillus anthracis* (4) and in fungal pathogens whereby MVs function as so-called "virulence bags" to deliver molecules that modulate the host cell response (5). For mycobacteria, there is a report of MV production by *Mycobacterium ulcerans*, which implies that vesicular transport and delivery systems are also found among mycobacteria (6). *Mycobacterium tuberculosis* (Mtb) infects a large proportion of the human population, yet only a small percentage of those infected develop clinically apparent disease (7). This epidemiological fact implies that most human hosts mount effective responses to Mtb that control infection. The innate immune response against Mtb begins with the inhalation of bacilli into the lungs where it is recognized by the pattern recognition receptors (PRRs) of alveolar macrophages, dendritic cells, and monocytes. Moreover, the internalization of the bacteria leads to the activation and rapid production of proinflammatory cytokines and chemokines along with other molecules, such as MMPs, which are involved in the recruitment of neutrophils, natural killer and T cells, and granuloma formation (8, 9).

Recognition of Mtb by PRRs is mediated primarily by TLRs, especially TLR2, TLR4, and TLR9 (10). In fact, the host immune response to Mtb in macrophages has been reported to be mediated primarily by TLR2 (10). Bacilli in macrophage phagosomes secrete abundant cell-surface components that include a surprisingly large number of TLR2 ligands, such as bacterial lipoproteins (19-kDa lipoprotein, LprA, and LprG) and the immunologically active glycolipids LAM, PIM_2, and PIM_6 (11–15). Paradoxically, the TLR2 interactions with the Mtb ligands can activate functions that promote the killing of the bacteria but also appear to be part of the bacterium's strategy to escape the host immune response. TLR2 lipid ligands traffic actively inside host macrophages and dendritic cells by incorporating into their endocytic networks and into exosomes (16). However, the mechanisms by which the bacilli shed these ligands are unknown.

Authorship note: Rafael Prados-Rosales and Andres Baena contributed equally to this work.

Conflict of interest: The authors have declared that no conflict of interest exists.

Citation for this article: *J Clin Invest.* 2011;121(4):1471–1483. doi:10.1172/JCI44261.

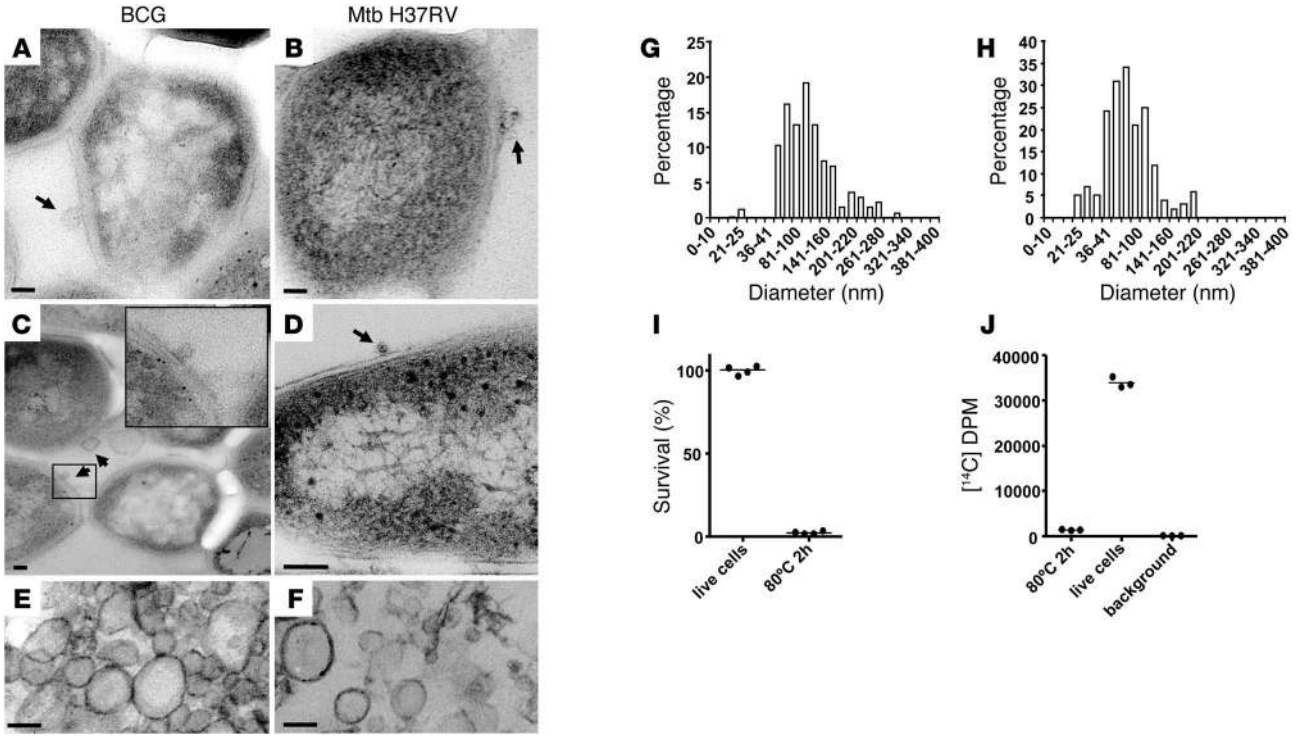

Figure 1

Dependence of MV production by mycobacteria on cell viability. TEM showing production of MVs by BCG (**A** and **C**) or Mtb strain H37Rv (**B** and **D**). In **A** and **B**, vesicles are seen budding from the surface of the bacteria (arrows). In **C** and **D**, arrows indicate vesicles that appear to have separated from the bacterial cell. The inset shows a vesicle associated to the bacterial surface. Scale bars: 50 nm. (**E** and **F**) TEM of MVs isolated from a day-14 culture of BCG (**E**) or Mtb H37Rv (**F**) grown in MM. Scale bars: 100 nm. The size distribution of isolated vesicles from BCG (**G**) or Mtb H37Rv (**H**) was determined by electron microscopy. (**I**) BCG cultures were labeled with ^{14}C-acetate (2 μCi ml^{-1}), harvested on day 5, and either left untreated or heat inactivated at 80°C for 2 hours. The viability of the cultures was determined by plating on 7H11 solid media at day 10, and percentage of survival was calculated by comparing CFU with bacterial particle counts obtained using a counting chamber. Each point represents an independent culture. (**J**) Cells prepared as described for **I** were resuspended in fresh medium and incubated for 5 additional days. The vesicle isolation procedure was carried out on supernatants from 3 independent cultures of heat-killed (80°C 2 hours) or live untreated BCG. The background level of radioactivity was determined isolating MVs on sterile medium containing ^{14}C-acetate (2 μCi ml^{-1}).

In this study, we have demonstrated MVs in many mycobacterium species, including the medically important *Mycobacterium bovis* bacillus Calmette-Guérin (BCG) attenuated vaccine strain and virulent Mtb. We show that mycobacterial MVs transport lipids and proteins previously known to be involved in the subversion of the immune response of the host. In addition, we demonstrate that these vesicles can trigger an inflammatory response in a TLR2-dependent manner that directly modulates the outcome of the interaction with the host, contributing to virulence and pathogenesis in Mtb infection.

Results

Release of MVs by multiple species of mycobacteria. We first investigated whether the *M. bovis* BCG and Mtb H37Rv strains release vesicles. We applied techniques developed for vesicle recovery from Gram-negative bacteria (17, 18) that used differential sedimentation and density gradient fractionation in an attempt to recover vesicles from mycobacterial culture supernatants. Transmission electron micrographic (TEM) analysis of pellets recovered from mycobacterial culture supernatants revealed vesicular structures associated to and pinching off the bacteria (Figure 1, A–D). The mass of this vesicular fraction was 250 μg ± 50 μg/l of minimal media (MM) (n = 4) and 135 μg ± 34 μg (n = 4) for BCG and Mtb, respectively. Electron micrographs revealed that more than 90% of the vesicles were closed forms (i.e., intact vesicles) (Figure 1, E and F), with diameters distributed between 60 and 300 nm (Figure 1, G and H).

Given that lipids released from dead or dying cells can self aggregate to form vesicles, we carefully assessed the viability of bacterial cultures from which vesicles were isolated and studied the effect of heat killing of the bacteria on vesicle generation. The viability of cells after 10 days of growth in 7H11 media was greater than 99%, as determined by comparing direct counts of bacterial particles with CFUs (Figure 1I). Although high viability argued against the vesicular material originating from dead cells, we could not completely exclude the possibility that vesicles originated from a minor fraction of dead or dying cells. Hence, we investigated alternate methods to establish an origin for the vesicles from live cells using metabolic labeling. Live and heat-inactivated mycobacterial cells previously radiolabeled with ^{14}C-acetate (Merck) (19) were suspended in fresh MM and incubated for 5 additional days. The extent of the heat inactivation was determined by counting CFUs on 7H11 media (Figure 1I). Vesicles were isolated and radioactivity was determined as the measure of lipid synthesis. The level of radioactivity found in material recovered from heat-inactivated cultures was similar to the background recovered from sterile medium, whereas it was significantly greater in super-

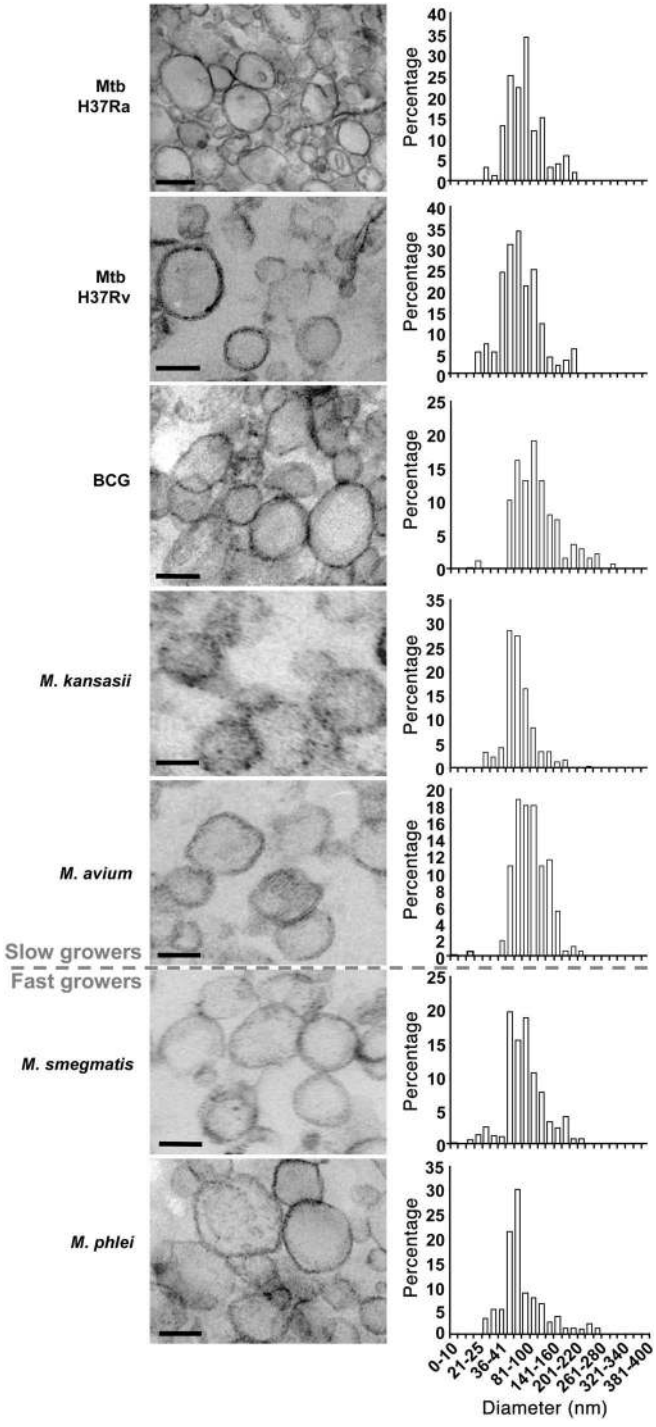

Figure 2
Vesicle production is conserved in the *Mycobacterium* genus. Vesicles were isolated from cultures inoculated with the indicated strains and visualized by TEM. The size distribution of the vesicles was determined by TEM. The pictures are representative of 5 independent experiments. Scale bars: 100 nm.

natants of cultures with live cells (Figure 1J). Furthermore, electron microscopy of mycobacteria revealed putative vesicles emerging from the bacterial cell wall with dimensions that were similar to isolated vesicles (Figure 1, A–D). We also investigated vesicle production in other mycobacterial species, including fast (*Mycobacterium smegmatis*, *Mycobacterium phlei*) and slow growers (*Mycobacterium avium*, *Mycobacterium kansasii*, and Mtb avirulent strain H37Ra) (Figure 2). All mycobacterial strains studied released vesicles in liquid cultures, and their size distribution as measured by TEM was similar, ranging from 40 to 250 nm in diameter (Figure 2).

Analysis of proteins associated with vesicles. To gain insight in the protein composition of MVs from both pathogenic (BCG and Mtb H37Rv) and nonpathogenic strains (*M. smegmatis*), vesicles were subjected to proteomic analysis using tryptic digestion prior to analysis by nano-LC-MS/MS. From 3 independent experiments, we identified 66 proteins in BCG, 48 in Mtb, and 64 in *M. smegmatis* vesicular preparations (Supplemental Tables 1–3; supplemental material available online with this article; doi:10.1172/JCI44261DS1). All proteins detected were classified according to the functional category given by the databases TubercuList v2.3, BoviList v3.1, and SmegmaList v1.0 (Figure 3A). Overall, BCG and Mtb MVs had similar protein compositions, while *M. smegmatis* MVs contained a markedly different set of proteins. In Mtb, most vesicular proteins were classified as belonging to "cell wall and cell processes" (38%) or "intermediary metabolism and respiration" (19%). Proteins annotated as being involved in "lipid metabolism" were detected at a lower frequency (4%). Similarly, MVs BCG proteins belonging to cell wall and cell processes also represented 37%. Conversely, in *M. smegmatis* MVs, this category contained only 8% of the proteins identified. MVs from BCG were enriched in the "lipid metabolism" category (21% vs. 4% for Mtb and 5% for *M. smegmatis*; Figure 3A and Supplemental Tables 1–3). Remarkably, both BCG and Mtb MVs showed a prominent component of lipoproteins representing 20% and 10% of the total proteins, respectively (Tables 1 and 2). Since lipoproteins typically represent between 1% and 2% of mycobacterial genomes (20), this represented a major enrichment in the MVs. In order to experimentally confirm this enrichment in lipoproteins in MVs of BCG and Mtb, we analyzed the protein profiles of cellular lysates of these bacteria grown under the same culture conditions that were used for generation of MVs (Supplemental Tables 4 and 5). We found that lipoproteins represented 1.4% and 2.6% of the total cell-associated proteins in BCG and Mtb, respectively. This result established that MVs from BCG and Mtb strains were enriched in lipoproteins, a finding consistent with active release. In contrast, no lipoproteins were found in *M. smegmatis* MVs, despite the fact that *M. smegmatis* has 68 putative lipoproteins in the genome, representing 1.03% of the total protein in *M. smegmatis* (Supplemental Table 6).

The proteomic approach was validated by demonstrating the presence of some of the proteins identified by MS with serological techniques. In this regard, DnaK, 19 kDa (Lpqh), and LprG were detected by immunoblot analysis of vesicular preparations (Figure 3B) and visualized by electron microscopy as vesicle associated by ImmunoGold electron microscopy (Figure 3C). Lipoproteins 19 kDa and LprG were located at the vesicle membrane, as expected from their lipidic nature. In contrast, DnaK localized to the lumen of the vesicles. We detected the presence of known secreted compounds such as LAM or α-glucan in the vesicle preparations by ELISA (Supplemental Figure 1A). Based on TEM images, LAM was detected both associated with the vesicles and unassociated, while α-glucan was clearly outside and apparently not associated with the vesicles (Supplemental Figure 1B). Since the molecular weight of α-glucan is around 100 kDa, it can be retained in the membrane

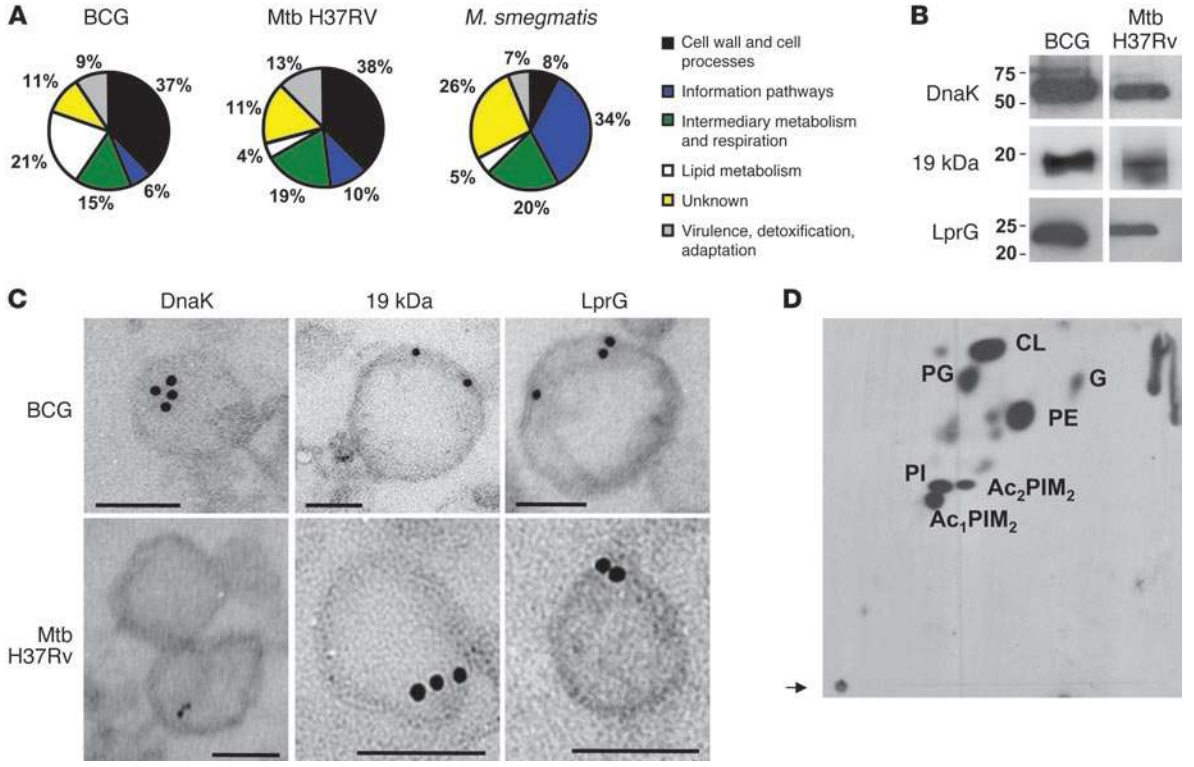

Figure 3

Mycobacterium vesicle–associated proteins and lipids. (**A**) Pie charts showing the BCG, Mtb, and *M. smegmatis* vesicle–associated proteins grouped into functional categories as in TubercuList, BoviList, and SmegmaList. Note that the "lipid metabolism" functional category is increased in BCG vesicles and that "cell wall and cell processes"–associated proteins are overrepresented in both BCG and Mtb compared with *M. smegmatis*. (**B**) Vesicles from the supernatant of the BCG culture were loaded onto a SDS-polyacrylamide gel, blotted on a nitrocellulose membrane, and incubated with mAbs with the indicated specificities. (**C**) ImmunoGold electron microscopy of thin sections of BCG and Mtb H37Rv vesicles treated with the mAbs specific for the indicated proteins and detected with a 10-nm IgG gold-labeled anti-mouse antibody. Scale bars: 100 nm. (**D**) Total lipids of vesicles isolated from ^{14}C-acetate–labeled cells were extracted with chloroform/methanol (2:1, v/v). Lipid extracts were separated by 2D TLC by applying an amount of lipids corresponding to 10,000 DPM per TLC plate and by using the solvent system E for separation of polar lipids. PG, phosphatidylglycerol; G, glycolipid; Ac_1PIM_2, monoacyl phosphatidylinositol dimannoside; Ac_2PIM_2, diacyl phosphatidylinositol dimannoside. Arrow indicates the origin.

used to concentrate the supernatants. Consequently, we analyzed the fractions recovered after Optiprep density gradient purification by Western blot for the presence of LAM and by ELISA for α-glucan (Supplemental Figure 1C). The 19-kDa lipoprotein was used as a vesicle marker, and the presence of this protein corresponded to fractions containing LAM. In contrast, the α-glucan was associated with the heaviest fractions of the gradient consisting of protein aggregates and polysaccharides. In summary, MVs from pathogenic mycobacteria were enriched in lipoproteins, some of them well-known TLR2 ligands, along with other major cell surface compounds such as LAM, but did not contain α-glucan.

Analysis of vesicle-associated lipids. To evaluate the lipid profile of the vesicles, we performed 2D-TLC analyses of total lipid extracts from BCG and H37Rv (data not shown) vesicles isolated from ^{14}C-acetate–labeled cultures. The vesicular lipids predominantly consisted of polar lipids (Figure 3D) with only low amounts of apolar lipids detectable (Supplemental Figure 2), consistent with the cell membrane being the likely origin of vesicles. The most abundant polar lipid species were phosphatidylinositol (PI) and acylated phosphatidylinositol dimannosides (PIM_2) along with cardiolipin (CL) and phosphatidylethanolamine (PE) (Figure 3D). To validate the 2D-TLC data, the BCG and Mtb vesicle samples were subjected to MALDI-TOF–MS analyses (Supplemental Figure 3). In addition to PI and acylated PIM_2, PIM_6 was also detected in the vesicle preparation. The results also showed that vesicles were enriched in polar lipids consistent with their origin from the cell membrane.

Production of MVs by BCG and Mtb during intracellular infection of macrophages in vitro and in vivo. The abundance of 19-kDa lipoprotein and LAM in vesicles provided an opportunity to use monoclonal antibodies to these components in immunoelectron microscopy for identification of vesicles in mycobacteria-infected macrophages in vitro and in vivo. This revealed vesicles shedding from the bacteria within phagosomes after 3 hours of infection (Figure 4A). In addition, MVs were seen trafficking at different locations in BCG-infected macrophages at 24 hours (Figure 4C). Similar findings were obtained with Mtb-infected macrophages at the same time intervals (Figure 4, B and D). To investigate whether the vesicle-release phenomenon could be documented in vivo, we infected mice with a high dose of CFSE-labeled bacteria. After 2 days, lungs were extracted and infected lung cells were sorted by FACS. Samples were processed for microscopy in the same manner as in vitro–infected macrophages and labeled with ImmunoGold. Images from this direct ex vivo analysis showed that BCG produced MVs within the phagosomes of macrophages that had been infected in vivo (Figure 4, E and F).

Table 1
BCG Pasteur vesicle–associated lipoproteins

GenBank no.	Name	MW (kDa)	No. unique peptides[A]	Mascot score[B]
gi|15610899	19-kDa lipoprotein antigen precursor LPQH	15.3	3	108
gi|31794050	Cell-surface lipoprotein MPB83	11.1	1	69
gi|31794222	FEIII-dicitrate–binding periplasmic lipoprotein	37.1	1	72
gi|31791596	Lipoprotein aminopeptidase LpqL	52.2	1	70
gi|31794122	Lipoprotein LppX	24.3	2	131
gi|31794183	Lipoprotein LppZ	39.1	1	70
gi|31791765	Lipoprotein LpqN	23.7	2	69
gi|31792462	Lipoprotein LprA	25	1	66
gi|31792564	Lipoprotein LprF	27	1	66
gi|31792605	Lipoprotein LprG	24.6	1	66
gi|31792123	Periplasmic phosphate-binding lipoprotein PSTS1 (PBP-1)	38.4	2	58
gi|31792115	Periplasmic phosphate-binding lipoprotein PSTS3	38	3	225
gi|31617703	phoS1	34.1	1	97

[A]Proteins identified with only 1 peptide were inspected manually. [B]Accurate identifications were considered when Mascot scores were above 45 ($P < 0.05$) for peptides or 51 ($P < 0.01$) for proteins.

Vesicles stimulated macrophages in a TLR2-dependent manner. To evaluate the capacity of mycobacterial MVs to trigger a proinflammatory response, we added BCG vesicle preparations to freshly isolated BMM from WT and TLR2-knockout mice and measured cytokine and chemokine expression at different times after vesicle addition (Figure 5A). The TLR1/2 ligand Pam_3CSK_4 was used as a positive control. The MVs induced the production of IL-1β, IL-6, IL-10, IL-12, TNF, CXCL1, and MIP-1α/CCL3, and the majority of these cytokines were induced in a TLR2-dependent manner, since their production from MV-stimulated *Tlr2*$^{-/-}$ cells was markedly reduced. However, induction of MIP-1α/CCL3 and IL-10 by MVs was preserved in *Tlr2*$^{-/-}$ cells, indicating that MVs also contained components that could activate macrophages through receptors different from TLR2. In contrast, Pam_3CSK_4 induced all cytokines and chemokines studied in a TLR2-dependent manner. We were able to detect cytokines as early as 3 hours after MV stimulation, and the response peaked at 24 hours. The induction of MIP-1α/CCL3 and IL-10 by MVs had faster kinetics than the other inflammatory mediators, consistent with induction through a different, non–TLR2-related mechanism. Levels of IL-12 and TNF were not completely abolished in the TLR2-deficient macrophages. The residual levels of TNF could have been due to an alternative pathway of activation involving MIP-1α (21). The fact that the majority of cytokines remained persistently elevated at 48 hours suggested a prolonged effect of the MV-associated ligands. Subsequently, we analyzed the levels of cytokines produced by macrophages stimulated with the same amount of *M. smegmatis* MVs at the same time points and found detectable levels of cytokines including IL-10, IL-12, and IL-1β, but their concentrations were significantly lower than observed with BCG MVs. In addition, no chemokines or TNF were detected for *M. smegmatis* MV-stimulated macrophages at any time point analyzed in the study (Supplemental Figure 6A).

The cyclooxygenase Cox-2 is known to regulate production of MMP-9 in a TLR2-dependent manner (22). Since vesicles were enriched in TLR2 ligands, we analyzed the levels of Cox-2 in WT and TLR2-deficient BMM and alveolar macrophages by Western blot (Figure 5B). Again, Pam_3CSK_4 was used as a positive control for TLR2 stimulation. BCG MVs triggered expression of Cox-2 in a time-dependent manner in WT BMM, whereas Cox-2 was not induced in macrophages from *Tlr2*$^{-/-}$ mice. The timing was very similar to that of induction of cytokines by MVs, with detectable levels appearing as early as 3 hours. The effect of MVs on Cox-2 expression was still present at 48 hours, indicating persistent stimulation by MVs as seen for cytokine secretion. Accordingly, the enhanced expression of Cox-2 protein resulted in increased levels of MMP-9 in the culture supernatants from BMMs stimulated with Pam_3CSK_4 or MVs, as measured by gelatin zymography (Figure 5B). The identity of the band was confirmed when the same experiment was carried out with BMMs from an *mmp-9*–knockout mouse, for which this gelatinolytic band was absent at 24 and 48 hours (Supplemental Figure 4). Neither Cox-2 nor MMP-9 was induced after stimulation of macrophages with *M. smegmatis* MVs (Supplemental Figure 6B). These results established that MVs from pathogenic mycobacteria were able to elicit production of a broad range of cytokines and other inflammatory mediators by macrophages in a TLR2-dependent manner.

Table 2
Mtb vesicle–associated lipoproteins

GenBank no.	Name	MW (kDa)	No. unique peptides[A]	Mascot score[B]
gi|15610899	19-kDa lipoprotein antigen precursor LPQH	15.3	3	134
gi|218661146	FEIII-dicitrate–binding periplasmic lipoprotein	37.1	1	63
gi|15610082	Lipoprotein LppX	24.3	1	79
gi|15608410	Lipoprotein LprA	25	2	118
gi|15608549	Lipoprotein LprG	24.6	2	138

[A]Proteins identified with only 1 peptide were inspected manually. [B]Accurate identifications were considered when Mascot scores were above 45 ($P < 0.05$) for peptides or 51 ($P < 0.01$) for proteins.

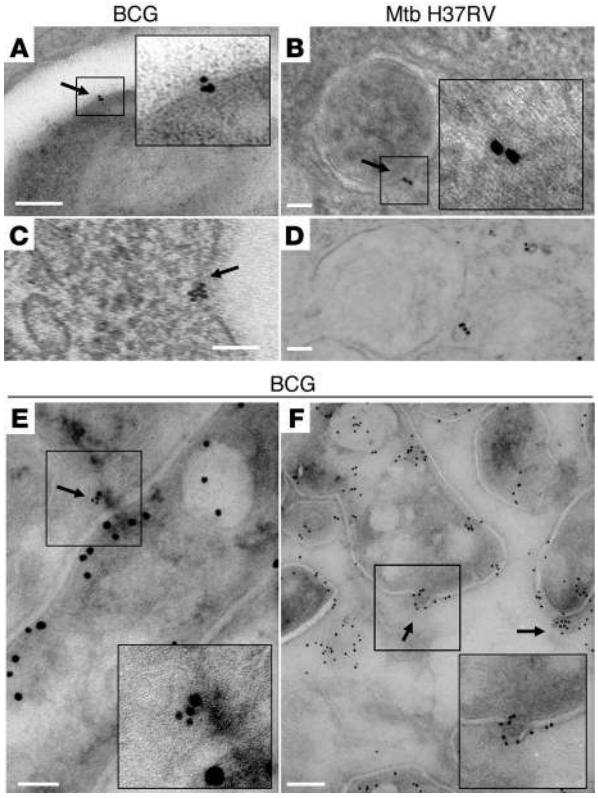

Figure 4
Production of vesicles by mycobacteria during intracellular infection of macrophages in vitro and in vivo. TEM showing MVs inside the BCG (**A** and **C**) or Mtb (**B** and **D**) in in vitro–infected macrophages at different time points after infection. Vesicles were observed by ImmunoGold labeling of sections with mAbs specific for 19-kDa lipoprotein (IT-12; 10 nm gold particles) and LAM (CS-35; 6 nm gold particles). (**A** and **B**) 19 kDa and LAM-labeled vesicles shedding from an intraphagosomal BCG (**A**) or H37Rv (**B**) after 3 hours of infection. (**C**) 19-kDa–labeled vesicle at the plasma membrane of a macrophage cell after 48 hours of in vitro infection with BCG. (**D**) TEM of a BMM infected in vitro with Mtb showing Mtb vesicles immunolabeled with IT-12 (10 nm) and CS-35 (6 nm) after 48 hours of infection. Scales bars: 50 nm. Pictures are representative of 2 independent experiments. (**E** and **F**) TEM of BCG in lung macrophages from infected mice revealing structures consistent with MV. As above, vesicles were observed by ImmunoGold labeling of sections with mAbs specific for 19 kDa (IT-12; 6 nm gold particles) and LAM (CS-35; 10 nm gold particles). Scale bars: 100 nm. Arrows indicate vesicles pinching off from the bacterial cell.

Stimulation of TLR2-dependent inflammatory responses in the lung by MVs. To evaluate the effect of MVs on tissue inflammatory responses and the role for TLR2 in such responses, we administered a single intratracheal (i.t.) injection of MVs to WT or TLR2-deficient mice and evaluated the lungs at different times for inflammatory responses. On the fifteenth day after MV infusion, the lungs of the WT mice showed marked alterations compared with PBS-infused controls, including dense areas of mononuclear cell infiltration and interstitial pneumonia (Figure 6). In addition, the MV-injected mice also showed a predominantly diffuse alveolar damage pattern of injury with more compaction of alveolar spaces. In contrast, no pathological changes were detected in TLR2-deficient mice. By day 23, the lesions in lungs of WT mice had worsened, but there was still little inflammatory change in the lungs of MV-injected TLR2-knockout mice, which appeared similar to the lungs of PBS-treated controls. Lung inflammation still occurred when lower doses of vesicles were administered (Supplemental Figure 7). Administration of the same amount of *M. smegmatis* MVs also triggered an inflammatory response at day 15 and day 23 (Supplemental Figure 6C), but it was not as intense as observed with pathogenic MVs (Figure 6).

Since myeloid cells are known to be recruited as mediators of inflammatory processes in the lungs, we next asked whether i.t. injection of MVs was associated with changes in the numbers and phenotypic subsets of these myeloid cells. To analyze this, total lung cell suspensions were analyzed for the expression of CD11b, CD11c, and Gr1 (Figure 7A). A significant increase in the absolute numbers of pulmonary $CD11b^{+}Gr1^{hi}$, $CD11b^{+}Gr1^{int}$, and $CD11b^{+}CD11c^{-}$ cells (Figure 7B) was observed in the MV-treated relative to the PBS-treated WT mice. These increases were not observed in the TLR2-deficient mice that received i.t. MVs. The increase in the total number of cells expressing the CD11b marker was also apparent by confocal microscopy at day 15 (Figure 7C). When *M. smegmatis* MVs were administrated, we observed a significant increase in the absolute numbers of pulmonary $CD11b^{+}Gr1^{hi}$ population only on day 15, no change in $CD11b^{+}Gr1^{int}$ or $CD11b^{+}CD11c^{-}$ cells, and decrease in $CD11b^{-}CD11c^{+}$ cells (Supplemental Figure 6D). These observations indicated that the vesicle treatment resulted in a profound alteration in the composition of the pulmonary myeloid populations in a TLR2-dependent manner. However, at day 23, only the $CD11b^{+}Gr1^{hi}$ cell population showed statistically significant differences (Supplemental Figure 5). Together, the above observations indicated that introduction of MVs into the lungs resulted in a profound alteration in the composition of the pulmonary myeloid populations in a TLR2-dependent manner.

Vesicles impaired the control of Mtb infection. Next, we investigated whether exposure to MVs modified the course of experimental Mtb infection. Mice received an i.t. injection of either MVs or PBS and 15 days later were infected via aerosol with a low dose of Mtb H37Rv. Lung histology was examined at 15 and 23 days after infection (Figure 8A). As expected, inflammatory infiltrates were observed in lungs of both groups of animals at day 15, but the MV-treated mice showed more discrete granulomatous structures, suggesting a more rapid progression of the inflammatory response. The difference between MV-treated and untreated mice was more pronounced at day 23, with MV-treated mice showing larger and more numerous granulomas compared with the PBS-treated control mice (Figure 8C). In contrast, the amount of inflammation observed for mice given *M. smegmatis* MVs at days 15 and 23 was significantly lower compared with that of the BCG-treated mice (Supplemental Figure 6E).

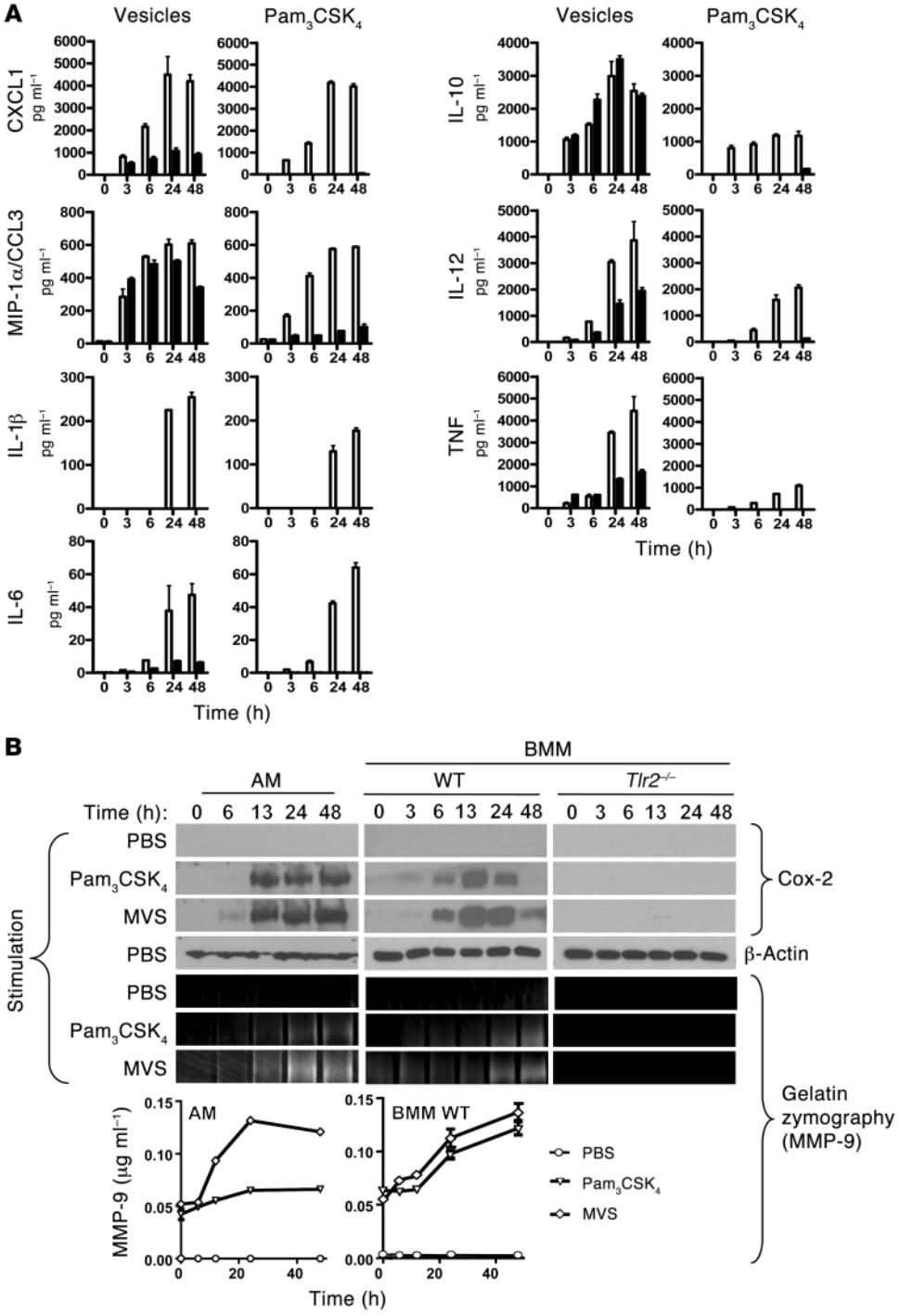

Figure 5
Responses of macrophages to BCG MVs. Freshly isolated BMM and alveolar macrophage cell line (AMJ2-C8) were stimulated with MVs and with Pam_3CSK_4 in vitro (500,000 cells/500 μl of media). Supernatants and cell lysates were collected at time points ranging from 0 to 48 hours after stimulation (*x* axes of all graphs indicate time in hours). (**A**) The supernatants of cultures of WT (white bars) or TLR2-knockout (black bars) isolated BMMs were assayed for cytokines IL-1β, IL-10, IL-12p70, TNF-α, and chemokines CXCL1 by multiplex ELISA (MSD Systems). Cytokines IL-6 and MIP-1α were analyzed by standard ELISA. Data represent mean ± SEM. (**B**) The levels of Cox-2 and MMP-9 were analyzed by Western blot and zymography, respectively. For Cox-2 analysis (top), lysates were made from cells (AMJ2-C8 alveolar macrophage cell line (AM), WT BMM, or *Tlr2*$^{-/-}$ BMM collected at the indicated times, ranging from 0 to 48 hours after addition of PBS (unstimulated), Pam_3CSK_4, or BCG MVs. For measurement of MMP-9 activity, culture supernatants were collected at the indicated times following stimulation as shown. The graphs at the bottom show levels of MMP-9 activity relative to a recombinant MMP-9 protein standard. The data of the Cox-2 and MMP-9 analysis are representative of 3 independent experiments. Data represent mean ± SEM.

We also studied BCG-vaccinated mice to determine whether vesicles can alter the outcome of the infection in animals with a recall response induced by previous vaccination (Figure 8B). The BCG-vaccinated mice that received MV injections showed markedly increased granulomatous inflammation (Figure 8B), and the number of granulomas per lung was higher compared with BCG-vaccinated mice that received only PBS injections (Figure 8C). The number of CFUs in the lung of unvaccinated mice at day 23 following Mtb infection was significantly higher in mice treated with vesicles (Figure 8D). This was also true when CFUs were counted in spleen (Figure 8E), suggesting that vesicles can promote the dissemination of the bacilli form the lung to other lymphoid organs. Similar trends were observed for BCG-vaccinated mice, although this did not reach statistical significance (Figure 8D). Conversely, the bacterial counts in the lung of mice treated with *M. smegmatis* MVs were significantly lower at day 23 compared with the PBS-treated mice, suggesting an alternative response that may be beneficial for the host (Supplemental Figure 6F) and indicating specificity in the inflammatory response triggered by pathogenic mycobacterial MVs.

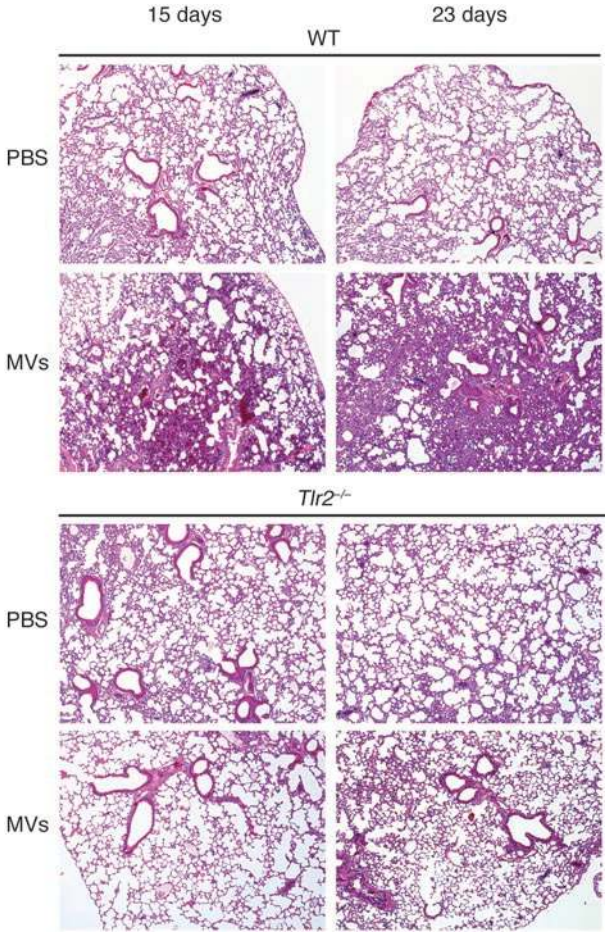

Figure 6
TLR2-dependent inflammation in mouse lungs after vesicle injection. Representative images of H&E-stained lung sections of i.t. vesicle or PBS-treated WT and *Tlr2*$^{-/-}$ C57BL/6 mice. Lungs were analyzed at 15 and 23 days after treatment. The images are representative of 5 lungs. All pictures were taken using a Coolscope (Nikon). The experiment was done twice. Original magnification, ×40.

Discussion

The present work represents the first study, to our knowledge, of production of MVs in 2 of the most clinically significant species of mycobacteria, *M. bovis* BCG and Mtb, along with other representatives of the mycobacterial genus including nonpathogenic strains. The results extend a prior report on vesicle production by *M. ulcerans* (6) and further define a newly recognized aspect of the host-pathogen interaction in mycobacterial infections with clear implications for pathogenesis, since MVs from nonpathogenic strains do not drive the same responses in the host. Furthermore, our results complement the observation that another Gram-positive bacterium, *B. anthracis*, produces MV (4), extending this mechanism into the subset of the Gram-positive group defined by the mycobacteria. Our results indicated that BCG and Mtb vesicles were physiologic products of live bacilli growing in liquid culture or within macrophages. Using different independent lines of experimentation, we showed that the production of vesicles by BCG depended on cell viability. Thus, vesicles were recovered only from live cultures, vesicle fractions were metabolically labeled only by live cells, and vesicular structures could be identified on the surface of mycobacteria in electron micrographs. Hence, we conclude that mycobacterial species, such as Gram-negative bacteria (1) and fungi (5), produce MVs that may facilitate the export of a variety of potential virulence factors.

The earlier study of vesicles released by *M. ulcerans* showed these to be enriched in mycolactone, a known toxin produced by this microorganism (6). This suggests that like many Gram-negative bacterial pathogens, mycobacteria produce MVs as carriers for virulence factors that modify the responses of host cells to infection (1). Consistent with this idea, our proteomic analyses of BCG, Mtb, and *M. smegmatis* MVs showed that only BCG and Mtb MVs were enriched in proteins associated with virulence, including a remarkably high content of putative TLR2 ligands such as the lipoproteins 19 kDa, LprA, and LprG. These molecules have been shown to downregulate the levels of MHCII molecules on macrophages and dendritic cells through a mechanism involving recognition by TLR2 (11–13). The lipid profile of BCG and Mtb MVs suggested that they originated from the bacterial cell membrane, since polar lipids typically found in the plasma membrane were the most abundant species. Interestingly, some of these polar lipids, such as PIM_2 or PIM_6, are known to be ligands of TLR2. As suggested by the nature of their protein and lipid cargo, mycobacterial MVs produced a profound TLR2-dependent inflammatory response in vitro and in vivo. In addition, MVs induced a range of inflammatory cytokines as well as the expression of key molecules implicated in early events of granuloma formation such as Cox-2 or MMP-9. Our in vivo studies indicated that MVs stimulated myeloid cell recruitment, leading to an increase in the $CD11b^{+}Gr1^{int}$ population subset in the lung. Remarkably, when vesicle-treated mice were challenged with Mtb H37Rv, they showed an increase in granulomatous inflammation in the lungs as well as an increase in the number of bacilli in both their lungs and spleens.

Mycobacterial lipids, including those originating from the cell wall, and proteins shed by phagocytosed mycobacteria are incorporated into released vesicles known as exosomes, which are produced by exocytic machinery of the mammalian host cells (16, 23). The way in which these surface compounds are released from the bacteria remains elusive. Given our observations using TEM showing the production of vesicles by the bacteria within the phagosomes of BMMs in vitro and in vivo and BMDCs (Rafael Prados-Rosales, unpublished observations), we propose that direct release by the bacteria of MVs provides a mechanism for transport of immunomodulatory compounds such as lipoproteins. This may lead to the distribution of these compounds to various compartments within infected host cells or to their incorporation into host cell–derived exosomes. Thus, generation and release of MVs may allow mycobacteria confined within phagosomes to deliver virulence factors to other cellular compartments or into the extracellular milieu to affect neighboring cells.

In addition to lipoproteins, our lipidomic studies showed that PI and PIM_2 along with CL and PE were the most prevalent polar lipids in MVs. Moreover, LAM was also detected as a part of the vesicles. LAM, lipomannan (LM), and PIMs are major lipoglycans that are noncovalently attached to the plasma membrane through their phosphatidyl-*myo*-inositol anchor and extend to the exterior of the cell wall (24). LAM is an important ligand in the interaction between Mtb and macrophages (25) and contributes to modulating the inflammatory response by downregulating IL-12 production (26). In addition, LAM inhibits phosphadityl inositol-3-phosphate

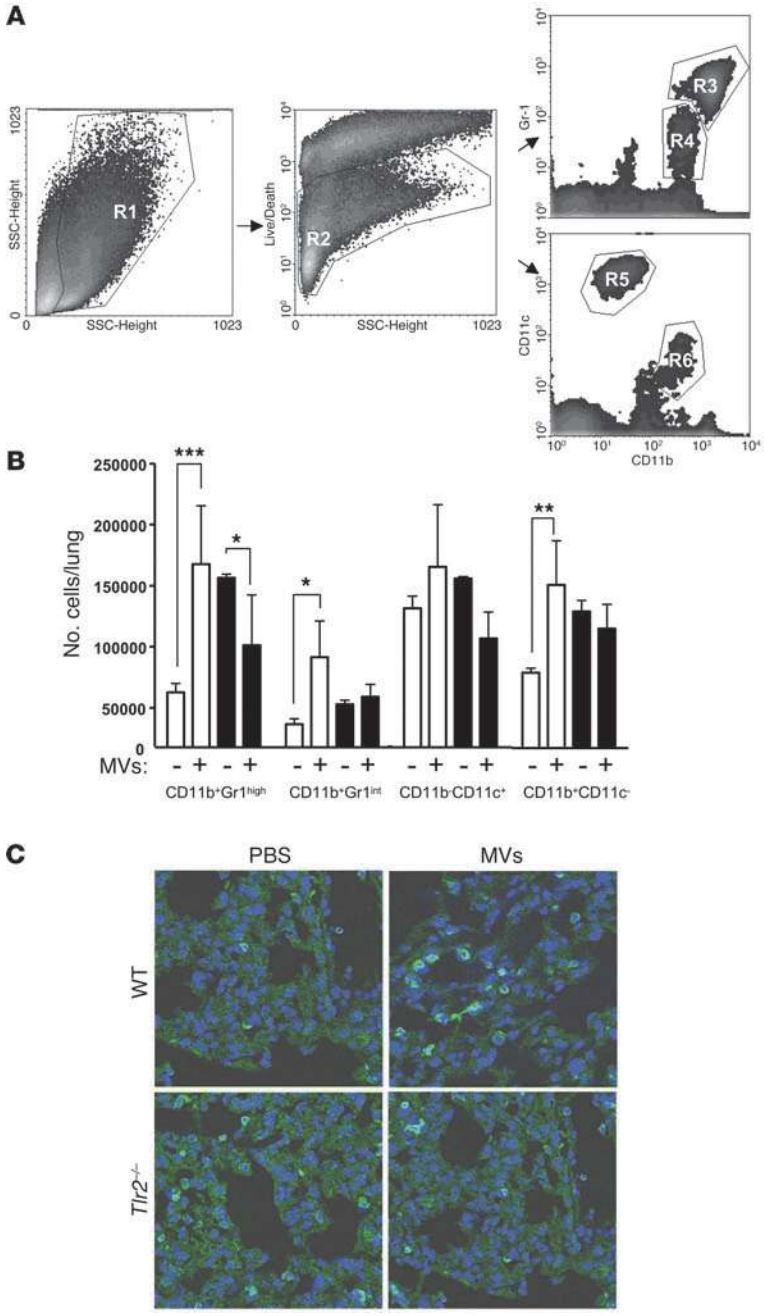

Figure 7

TLR2-dependent increase in myeloid cells in the lungs following i.t. MV injection. (**A**) Representative flow cytometry dot plots showing the gating for analysis of different myeloid populations (R3, $CD11b^+Gr1^{hi}$; R4, $CD11b^+Gr1^{int}$; R5, $CD11b^-CD11c^+$; and R6, $CD11b^+CD11c^-$). (**B**) Bar graphs indicating the mean absolute numbers of the different populations of lung cells of WT (white bars) and *Tlr2*$^{-/-}$ (black bars) mice. Data represent mean ± SEM. $^*P < 0.05$; $^{**}P < 0.01$; $^{***}P < 0.001$. (**C**) Confocal inmmunofluorescence microscopy of cryosections stained with DAPI and CD11b–Alexa Fluor 647 showing an increase in $CD11b^+$ cells after vesicle treatment at 15 days in WT but not in the *Tlr2*$^{-/-}$ mice. Data are representative of 2 independent experiments.

(PI3P) association with Mtb phagosomes (27) and blocks calcium flux in infected cells (28). Conversely, LM and PIMs can induce a proinflammatory response by inducing TNF-α, IL-8, and IL-12 secretion (29). Other important mycobacterial cell wall components, such as the glycolipid trehalose dimycolate (TDM), have been implicated in the development of an inflammatory response and in granuloma formation (30, 31). However, we did not find TDM associated with MVs in our 2D-TLC analysis. Recently, mycobacterial PIM_2 was reported to induce the expression of Cox-2 and subsequently MMP-9 in a TLR2-dependent manner (22), which parallels our findings in cells exposed to isolated MVs. These enzymes modify the host response, as Cox-2 generates prostaglandins that modulate the cell death response to infection (32) and MMP-9 is a metalloprotease known to be involved in the remodeling of the extracellular matrix during the early events of granuloma formation (33, 34). We did not explore the contribution of other TLRs, such as TLR4, TLR6, or TLR9, which have been shown to have a role in the recognition of Mtb in mice and human (35–38). However, we detected DNA in purified and intact mycobacterial MVs (our unpublished data), suggesting a possible interaction of MVs with TLR9.

One of the key features of mycobacterial infections is the production of an inflammatory Th1 response that promotes the secretion of selected cytokines such as TNF-α, INF-γ, and IL-12 (39, 40). However, our analysis of cytokines produced by BMMs stimulated with MVs did not indicate the induction of a typical Th1 priming milieu, since cytokines that oppose Th1 priming such as IL-10 were also induced (41). IL-10 has been shown to block activation of macrophages, which may increase the dissemination of the bacteria. In addition, the chemokines CXCL1 and CCL3 were induced in BMMs by MVs, which along with other cytokines are critically involved in recruitment of multiple effector cells at the site of infection. The analysis of the type of myeloid cells recruited after a BCG MV treatment showed an increase in the $CD11b^+Gr1^{hi}$, $CD11b^+$ $Gr1^{int}$, and $CD11b^+CD11c^-$ cell populations. This is relevant because a strong inflammatory response and an increase in the cell population $CD11b^+Gr1^{int}$ have been recently associated with progression of tuberculosis (42), providing support for the hypothesis that MVs contribute to the virulence of *Mycobacterium*. Moreover, this population has been shown to be permissive for mycobacterial replication in mice (43). Although more phenotypic markers are required to define this $CD11b^+Gr1^{int}$ population, we believe that they may be a subset of myeloid-derived suppressor cells (MDSC), which may have inhibitory properties in the context of infection by intracellular bacterial pathogens, including Mtb (44). Remarkably, this $CD11b^+Gr1^{int}$ myeloid cell population did not increase upon treatment with *M. smegmatis* MVs, suggesting that its recruitment may be specifically associated with pathogenic mycobacteria. We note that there is increasing evidence that macrophage and dendritic cell responses to microbial antigens can differ (45) and the interaction of vesicles with dendritic cells should be a priority for future studies.

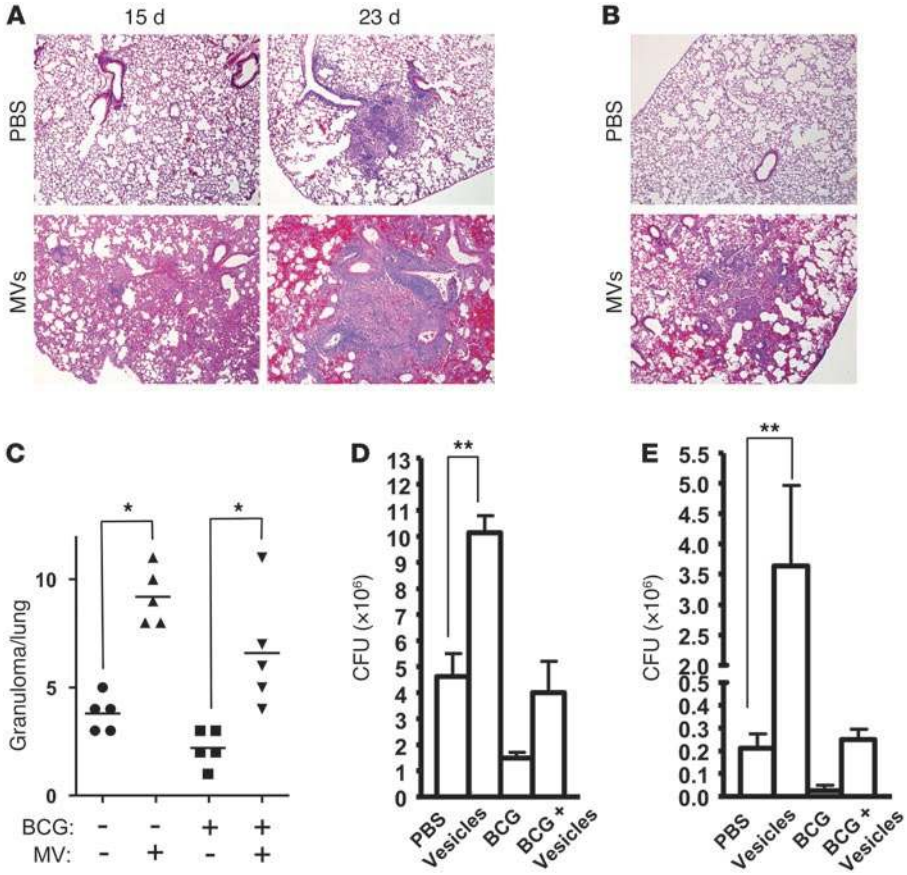

Figure 8
Exacerbation of mycobacterial infection by pretreatment with isolated vesicles. (**A**) Representative images of H&E-stained lung sections of mice that received i.t. infusion of purified BCG MVs or PBS, followed by aerosol challenge with Mtb H37Rv 15 days later. Lungs were analyzed at 15 and 30 days after challenge. (**B**) Representative images of H&E-stained lung sections of BCG-vaccinated WT C57BL/6 mice infused with vesicles or PBS and challenged with a low dose of H37Rv (50–100 CFUs). Mice were vaccinated with BCG by intradermal injection and 6 weeks later received i.t. PBS (control) or purified BCG MVs. Aerosol challenge with MTb H37Rv was done 15 days later. Lungs were analyzed at 30 days after the challenge. All pictures were taken using a digital camera Coolscope (Nikon). Original magnification, ×40. (**C**) Quantification of the number of granuloma per lung in mice receiving the indicated treatments followed by Mtb H37Rv challenge. Analysis was done at day 30 after challenge. (**D** and **E**) CFUs in lungs (**D**) and spleens (**E**) of mice receiving the indicated treatments followed by Mtb H37Rv challenge. Analysis was done at day 30 after challenge. Experimental data are representative of 2 independent experiments. Data represent mean ± SEM. $^{**}P < 0.01$.

Our findings point to MVs as a factor that is detrimental for the host during Mtb infection. In support of this, we note the observations that mice pretreated with pathogenic MVs developed a more acute inflammation and higher bacterial loads in the lungs compared with control and nonpathogenic MV-treated mice and that preexposure to MVs also increased dissemination of bacilli from the lung to other lymphoid organs such as the spleen. Furthermore, we observed MVs in mycobacteria recovered from mice, providing evidence for the formation of these structures in vivo and lending support to the view that MVs represent a bacterial release mechanism relevant to pathogenesis.

In summary, we have confirmed the existence of a vesicular system in mycobacteria and demonstrate that the vesicles produced contain numerous components associated with virulence. The finding that MVs are released inside macrophages in vivo suggests that they have the capacity to influence the outcome of the macrophage-mycobacteria interaction. Mycobacterial vesicles are proinflammatory through a TLR2-dependent mechanism, providing additional evidence for the key role of the innate immune receptor in host defense against Mtb. The work reported in the current study raises many important questions about the relevance of MVs to the adaptive immune response against Mtb, which ultimately may be resolved through the isolation of bacterial mutants that are deficient in vesicle production. The discovery of a vesicular transport system in mycobacteria opens up new horizons for the pathogenesis of tuberculosis and vaccine development.

Methods

Mycobacteria and bacterial culture. *M. bovis* BCG (Pasteur strain) and other mycobacteria (Mtb strains H37Rv [virulent] and H37Ra [avirulent], *M. kansasii*, *M. phlei*, *M. smegmatis*, and *M. avium*) were grown in an MM consisting of 1 g/l KH_2PO_4, 2.5 g/l Na_2HPO_4, 0.5 g/l asparagine, 50 mg/l ferric ammonium citrate, 0.5 g/l $MgSO_4 \times 7\ H_2O$, 0.5 mg/l $CaCl_2$, 0.1 mg/l $ZnSO_4$, with or without 0.05% tyloxapol (v/v), containing 0.1% (v/v) glycerol, pH 7.0. In some experiments as stated, cultures were grown in Middlebrook 7H9 medium (M7H9) supplemented with 10% (v/v) OADC enrichment (BD Microbiology Systems), 0.5% (v/v) glycerol, and with or without tyloxapol 0.05% (v/v; Sigma-Aldrich). Cultures were grown for up to 10 days as indicated in roller bottles at 37°C. To study the requirement for cell viability, mycobacterial precultures were used to inoculate fresh MM supplemented with 1 μCi ml^{-1} [1,2-^{14}C]-acetate (50–62 mCi $mmol^{-1}$; Merck). Cultures were harvested at day 5 and bacterial cells were killed by heating to 80°C for 2 hours. After this, live cells and heat-killed cells were again inoculated in fresh MM and incubated for 5 additional days at 37°C. Vesicles were then isolated and radioactivity measured in a scintillation counter. To assess cell viability at day 10, number of cells was determined directly by manual counting using a Petroff-Hausser Counting Chamber and standard microscope with ×40 magnification and then compared with the number of CFUs obtained by plating serial dilutions on 7H11 agar media.

Vesicle isolation and purification. Vesicles were isolated as described with minor modifications (17). The basic protocol involved a combination of serial differential sedimentation and density gradient purification. Briefly, cells were pelleted (3,450 *g* for 15 minutes, 4°C) from 1000 ml cultures and the supernatants were filtered through a 0.45-mm–pore size polyvinylidene difluoride filter (Millipore). The supernatant volumes were

then concentrated approximately 20-fold using an Amicon Ultrafiltration System (Millipore) with a 100-kDa exclusion filter. The concentrate was then sequentially centrifuged at 4,000 and 15,000 *g* (15 minutes, 4°C) to remove cell debris and aggregates, and the remaining supernatant was then centrifuged at 100,000 *g* for 1 hour at 4°C to sediment the vesicular fraction into a pellet. The supernatant was then discarded, the pellet was suspended in 1 ml of 10 mM HEPES, 0.15 M NaCl, and mixed with 2 ml of Optiprep solution (Sigma-Aldrich) in 10 mM HEPES and 0.15 M NaCl (yielding 35% [w/v] Optiprep final concentration). The crude vesicle sample was then overlayed with a series of Optiprep gradient layers with concentrations ranging from 30%–35% (w/v). The gradients were centrifuged (100,000 *g*, 16 hours), and 1 ml fractions were removed from the top. The fractions were then dialyzed separately in PBS overnight and again recovered by sedimentation at 100,000 *g* for 1 hour. Finally, the vesicles were suspended in LPS-free PBS. For quantitation of vesicles, aliquots of preparations isolated from MM were stained with CFSE (Invitrogen) at 10 μM final concentration in PBS for 30 minutes at 37°C. After 2 washes in PBS, labeled vesicles were diluted and counted by fluorescence microscopy (Axiovert 200M; Carl Zeiss Inc.). Fluorescent images consisted of 1344 × 1024 pixels and were taken at ×40 (0.101 μm × pixel). The concentration of vesicles was calculated as a function of the field area and then corrected for the loaded volume. Five different fields were counted.

Electron microscopy. TEM was used to analyze the morphology and integrity of extracellular vesicles isolated from culture supernatants and to visualize the interaction of MVs with mycobacteria and macrophages. MVs were fixed with 2% glutaraldehyde in 0.1 M cacodylate at room temperature for 2 hours and then incubated overnight in 4% formaldehyde, 1% glutaraldehyde, and 0.1% PBS. After fixation, the samples were stained for 90 minutes in 2% osmium, then serially dehydrated in ethanol and embedded in Spurrs epoxy resin. Thin sections were obtained on an Ultracut UCT (Reichert) and stained with 0.5% uranyl acetate and 0.5% lead citrate (Reichert). Samples were observed in a JEOL 1200EX transmission electron microscope operating at 80 kV. For ImmunoGold labeling of BCG- or H37Rv-infected macrophages or vesicles, samples were first fixed in 0.1 M sodium cacodylate buffer (pH 7.2) containing 4% paraformaldehyde, 0.2% glutaraldehyde, infiltrated in 25% polyvinylpyrrolidone and 2.1 M sucrose and then rapidly frozen by immersion in liquid nitrogen. Cryosections were obtained in a temperature range of −70 to −90°C using an Ultracut UCT. After blocking with PBS-BSA with 50 mM NH_4Cl, the cryosections were incubated overnight in the presence of the mouse monoclonal antibodies specific for DnaK (IT-42; IgG1), lipoprotein 19 kDa (IT-12; IgG1), lipoprotein LprG (Rv1411, IgG1), LAM (CS-35, IgG1), or α-glucan (24c5; IgG1; ref. 46). After incubation with ImmunoGold-labeled anti-mouse IgG, specimens were observed in a JEOL 1200EX transmission electron microscope operating at 80 kV.

Protein identification by liquid chromatography-tandem mass spectrometry. Proteins were precipitated from vesicle suspensions and bacterial lysates by adding 6 volumes of ice-cold acetone and the pellets dissolved in 25 mM ammonium bicarbonate. Proteins were reduced with 10 mM DTT at room temperature for 1 hour, and the cysteine residues were subsequently alkylated with 10 mM iodoacetamide at room temperature for 1 hour in the dark. Protein digestion was carried out with trypsin (Promega, 1:20; w/w) at 37°C for 16 hours. The peptide mixtures from in-solution tryptic digestions were analyzed using Nanoflow LC-MS/MS. The peptides were loaded onto a 0.3 × 5 mm C18 precolumn (New Objective) and then eluted with a linear gradient of 2%–90% acetonitrile in 0.1% aqueous solution of formic acid. The gradient was delivered over 120 minutes by a NanoLC 1D Plus (Eksigent) at a flow-rate of 200 nl/min, through a 75-μm × 15-cm fused silica capillary C18 HPLC PepMap column (LC Packings) to a stainless steel Nanobore emitter (Proxeon). The peptides were scanned and fragmented with an LTQ XL linear ion trap mass spectrometer (ThermoFinnigan) operated in data-dependent and MS/MS switching mode using the 3 most intense precursors detected in a survey scan from 400 to 1600 amu (3 μscans). Normalized collision energy was set to 35%, and dynamic exclusion was applied during 3-minute periods to avoid repetitive fragmentation of ions. Generated .raw files were converted to .dta files for Mascot database. A database containing the NCBInr Bacteria sequences (9,940,348 sequences, as of April 15, 2010) was searched using Mascot Software (version 2.3; Matrix Science) for protein identification. Search criteria included trypsin specificity with 1 missed cleavage allowed and methionine oxidation as variable modification. Search criteria included (a) trypsin specificity with 1 missed cleavage allowed, (b) methione oxidation as variable modification, and (c) a minimum precursor and fragment-ion mass accuracy of 1.2 and 0.3 Da, respectively, and a requirement of at least 1 bold red peptide (i.e., highest scoring peptide matching to protein with highest total score). Cut-off values for Mascot scores of peptides and proteins were set to 45 ($P < 0.05$) and 51 ($P < 0.01$), respectively, for consideration as accurate identifications. Proteins identified with only 1 peptide were inspected manually. The false-positive rate (1.68%) was calculated searching the same spectra against the NCBInr Bacteria decoy database, using the version updated April 15, 2010. A combined list of proteins identified in all replicates was condensed in order to remove redundant IDs such as orthologous sequences, redundant database entries, and indistinguishable isoforms based on observed peptide coverage.

Vesicle-associated protein analysis. Proteins (5 μg) of MVs and mycobacterial fractions were separated with 12% SDS-PAGE, and gels were stained with Coomassie blue. To validate the proteomic approach, the presence of some proteins of interest in the vesicle preparation was confirmed by Western blot. Proteins were transferred to nitrocellulose membranes and blocked with 5% (w/v) nonfat dry milk in PBS for 1 hour at room temperature before incubating with the mAbs specific for DnaK (IT-42; IgG1, BEI Resources), 19-kDa lipoprotein (IT-12; IgG1, BEI Resources) and LprG (Rv1411; IgG1, BEI Resources) overnight at 4°C. After washing with PBS plus 0.05% Tween-20 (PBST), the membranes were incubated with an anti-mouse IgG (H+L) HRP (Invitrogen) as a secondary antibody for 1 hour. The immunoreactive bands were visualized with a chemiluminescent substrate.

Vesicle-associated lipid analysis. Total lipids of vesicles isolated from ^{14}C-acetate–labeled cells (2 μCi ml^{-1}) for 12 days were extracted with chloroform:methanol (2:1; v/v). Lipid extracts were separated by a series of 2D TLC systems as previously published (47) by applying equal amounts of lipids corresponding to 10,000 DPM per TLC plate and by using the solvent systems A–D for separation of apolar lipids and E for separation of polar lipids, respectively. MALDI-TOF mass spectrometry analysis of lipids was performed as previously described (48).

Cox-2 and MMP-9 analysis. Macrophage lysates were separated by SDS-PAGE and then transferred electrophoretically to PVDF membranes. The blots were blocked with 5% (w/v) nonfat dry milk in PBS for 1 hour at room temperature and subsequently incubated overnight at 4°C with a Cox-2–specific primary antibody (Cayman) in PBST with 5% (w/v) nonfat dry milk. Following 3 washes of 5 minutes each with PBST, the blots were incubated with horseradish peroxidase–conjugated goat anti-rabbit IgG (Southern Biotech) in blocking buffer for 1 hour at room temperature. After 3 washes with PBST, the blots were developed by chemiluminescence using the ECL-pico Western Detection Kit (Pierce) and exposed to x-ray film (Kodak XAR5).

Measurement of MMP-9 activity was done by measurement of gelatin hydrolysis within SDS-PAGE gels (34). For MMP-9 analysis, conditioned cell culture medium was removed and mixed with nonreducing 5× sample buffer. The mix was incubated at 37°C in a water bath for 20 minutes. Samples were electrophoresed on 7.5% (w/v) nonreducing SDS-PAGE gels containing 0.1% (w/v) gelatin as a substrate. The gels were first incubated on a rotating platform in TBS containing 2.5% Triton X-100 for 120 minutes to remove SDS and then in TBS alone for

10 minutes. Finally, gels were incubated in 5 mM $CaCl_2$, 150 mM NaCl, and 0.01% Triton X-100 for 18 hours at 37°C. Gelatinolytic activity was visualized as clear areas in the Coomassie blue–stained gel. Recombinant mouse MMP-9 (R&D Systems) was used as a standard for the assay. Quantification of MMP-9 activity in gels was done by comparing the pixel intensity of the white areas in the gel.

Mouse immunizations and infections. C57BL/6 female mice between 6 and 8 weeks old were purchased from Jackson Laboratories. All procedures involving mice were reviewed and approved by the Animal Use and Care Committee of the Albert Einstein College of Medicine. Animals were maintained in a specific pathogen–free animal facility under animal biosafety level 2 conditions for all experiments, except for those involving infection with virulent Mtb, for which animal biosafety level 3 conditions were used. TLR2-deficient mice on a C57BL/6 background were a gift of S. Akira (49). For i.t. immunization, anesthetized mice received an i.t. injection of 25 μg of vesicles in 50 μl of PBS, corresponding to 2×10^8 vesicles according to previously published methods (9). Control mice received i.t. injections of PBS. Aerogenic challenge was done using a whole-body exposure aerosol chamber (Mechanical Engineering Workshop) custom fitted to a class 3 biosafety cabinet (Baker) to deliver 10–50 CFU per animal of Mtb (H37Rv). For BCG immunizations, each mouse received s.c. 1×10^6 CFUs. Mice were euthanized at 15 or 30 days after challenge. Lungs and spleens of individual mice were aseptically removed and homogenized separately in 5 ml PBS plus 0.05% tyloxapol using a Seward Stomacher 80 blender (Tekmar). The homogenates were diluted serially and plated on Middlebrook 7H11 agar to determine CFU of Mtb. The number of granuloma per lung was assessed by counting 4 sections from each lung cut at intervals of 100 μm in depth at a magnification of ×40. Pictures were taken using a digital camera COOLSCOPE (Nikon). Five lungs per treatment were analyzed.

BM macrophages. BM macrophages (BMMs) were derived from the femur and tibia of mice, as described (50). Briefly, leg bones were removed and the attached muscle tissue was removed. After disinfection in 70% ethanol, both ends were cut and the marrow flushed with PBS using a syringe with a 0.45-mm diameter needle. At day 0, BM precursors were seeded at 2×10^6 per 100-mm dish in 10 ml complete medium (DMEM; Gibco, Invitrogen, supplemented with decomplemented 10% FCS, L-glutamine, HEPES, β_2-mercaptoethanol, and penicillin/streptomycin) with 20% conditioned medium (containing M-CSF) isolated from a L929 fibroblast cell line culture (50). The BMM were harvested at day 7 for use in experiments.

Cytokine ELISAs. Macrophage culture supernatants were assayed for a panel of mouse Th1/Th2 cytokines and chemokines using a 9-plex multiplex ELISA system that uses signal development based on an electrochemiluminescence reaction (Mesoscale Discovery Systems Inc.), according to the manufacturer's specifications. The cytokines IL-6 and MIP-1α were analyzed using standard capture ELISAs (from BD Biosciences and R&D Systems, respectively) according to the manufacturers' instructions.

Macrophage infections. Monolayers of BMMs (5×10^5 cells) were infected with BCG or Mtb H37Rv at an MOI of 10:1 or treated with 4.5×10^7 vesicles. After 3 hours, cells were treated with gentamicin (100 μg/ml; Life Technologies) for 1 hour to inhibit the growth of extracellular bacteria, and the cells were then washed 2 times with PBS and cultured in fresh medium containing 20 μg/ml of gentamicin. Cells were collected at different time intervals (3, 6, 24, and 48 hours) after infection and processed for analysis. At the same time intervals, cell-free supernatants were collected and stored at –80°C until assayed for cytokines by ELISA or for MMP-9 activity by gelatin zymography.

Histological analysis. The lungs were removed aseptically from mice, fixed in 10% buffered formalin phosphate (Fisher), and embedded in paraffin. Serial 4-μm sections were cut and stained with H&E. For immunohistochemistry, lungs were fixed with 2% paraformaldehyde in PBS for 2 hours at 4°C. After fixation, the tissues were transferred and incubated in 30% sucrose overnight at 4°C. Tissues were then embedded in OCT (Sakura Finetek USA Inc.) and frozen in –70°C isopentane. Sections of 4-micron thickness were cut and stained with Alexa Fluor 647–labeled anti-CD11b and DAPI. Staining was analyzed using a LEICA SP5 confocal microscope (Leica Inc.) and Leica LAS-AF software.

Analysis of lung cell populations. The composition of lung inflammatory infiltrates was analyzed by flow cytometry. Briefly, lungs were perfused with heparin in DMEM after excision and incubated with 0.4 mg/ml Liberase CI solution (Roche Biochemicals) and DNase I for 1 hour at 37°C. Single-cell suspensions were prepared by gently pressing the tissue through a 70-μm nylon mesh cell strainer with a syringe plunger. Red cells were lysed for 5 minutes in 3 ml of erythrocyte lysis buffer (Sigma-Aldrich) diluted 1:1 with PBS. Cells were centrifuged and resuspended in FACS buffer (2% FCS, 0.05% sodium azide in PBS). Clumps were removed by passing the cell suspensions through a 50-μm cell strainer. To analyze the phenotype of pulmonary subpopulations, cell suspensions were first blocked with 2.4G2 mAbs to block Fc receptors and then stained with LIVE/DEAD dye (Invitrogen) followed by staining with fluorochrome-conjugated mAbs specific for CD11b (Alexa Fluor 647; eBioscience), CD11c (PE; BD Biosciences), and Gr1 (FITC; BD Biosciences). The FACS data was analyzed using WinMDI 2.9 (free software; Scripps Institute).

Analysis of production of MVs in vivo. *M. bovis* BCG Pasteur was stained with CFSE (Invitrogen) at a 10-μM final concentration in PBS for 30 minutes at 37°C. Cells were washed extensively in PBS plus 0.05% tyloxapol (Sigma-Aldrich), and OD was measured at 600 nm. An amount corresponding to 5×10^7 CFSE-labeled bacteria was injected intravenously into mice by the lateral tail vein. Two days later, mice were sacrificed and lungs were extracted and processed as above to obtain a single-cell suspension. Lung cells were sorted using a high-speed cell sorter (MoFlo; DAKO-Cytomation) with gating on CFSE-positive cells. Samples were further submitted to ImmunoGold labeling and cryosectioning for TEM analysis as above.

Statistics. ANOVA was used to assess statistical significance of differences in the means. Student's *t* test (2-tailed) was applied for experiments involving pairwise comparisons. $P \leq 0.05$ was considered significant.

Acknowledgments

A. Casadevall is supported by NIH awards HL059842, AI033774, AI052733, AI033142, and the AERAS foundation for vaccine development. A. Casadevall is also supported by the Northeastern Biodefense Center under grant U54-AI057158-Lipkin. S.A. Porcelli and W.R. Jacobs Jr. were supported by the NIH Program Project grant AI-063537. R. Kalscheuer acknowledges support from the Juergen Manchot Foundation. Flow cytometry studies were carried out using core facilities supported by the Einstein Cancer Center (NIH/NCI CA013330) and the Einstein Center for AIDS Research (NIH AI-51519). Special thanks are given to C.A. Duque and V. Cabezon for their helpful discussion, support, and inspiration.

Received for publication July 6, 2010, and accepted in revised form January 5, 2011.

Address correspondence to: Arturo Casadevall, Albert Einstein College of Medicine, Jack and Pearl Resnick Campus, 1300 Morris Park Avenue, Forchheimer Building, Room 411, New York, New York 10461, USA. Phone: 718.430.2811; Fax: 718.430.8771; E-mail: casadeva@aecom.yu.edu.

Luis Martinez's present address is: Long Island University-C.W. Post, Department of Biomedical Sciences, Brookville, New York, USA.

1. Kuehn MJ, Kesty NC. Bacterial outer membrane vesicles and the host-pathogen interaction. *Genes Dev*. 2005;19(22):2645–2655.
2. Deatherage BL, Lara JC, Bergsbaken T, Rassoulian Barrett SL, Lara S, Cookson BT. Biogenesis of bacterial membrane vesicles. *Mol Microbiol*. 2009; 72(6):1395–1407.
3. Beveridge TJ. Structures of gram-negative cell walls and their derived membrane vesicles. *J Bacteriol*. 1999;181(16):4725–4733.
4. Rivera J, Cordero RJ, Nakouzi AS, Frases S, Nicola A, Casadevall A. Bacillus anthracis produces membrane-derived vesicles containing biologically active toxins. *Proc Natl Acad Sci U S A*. 2010;107(44):19002–19007.
5. Rodrigues ML, et al. Extracellular vesicles produced by Cryptococcus neoformans contain protein components associated with virulence. *Eukaryot Cell*. 2008;7(1):58–67.
6. Marsollier L, et al. Impact of Mycobacterium ulcerans biofilm on transmissibility to ecological niches and Buruli ulcer pathogenesis. *PLoS Pathog*. 2007;3(5):e62.
7. Bloom BR, Fine PEM. The BCG experience: Implications for future vaccines against tuberculosis. In: Bloom BR, ed. *Tuberculosis, Pathogenesis, Protection and Control*. Washington, DC, USA: American Society for Microbiology Press; 1994:531–557.
8. Davis JM, Ramakrishnan L. The role of the granuloma in expansion and dissemination of early tuberculous infection. *Cell*. 2009;136(1):37–49.
9. Feldmesser M, Casadevall A. Effect of serum IgG1 to Cryptococcus neoformans glucuronoxylomannan on murine pulmonary infection. *J Immunol*. 1997;158(2):790–799.
10. Jo EK, Yang CS, Choi CH, Harding CV. Intracellular signalling cascades regulating innate immune responses to Mycobacteria: branching out from Toll-like receptors. *Cell Microbiol*. 2007;9(5):1087–1098.
11. Brightbill HD, et al. Host defense mechanisms triggered by microbial lipoproteins through toll-like receptors. *Science*. 1999;285(5428):732–736.
12. Pecora ND, Gehring AJ, Canaday DH, Boom WH, Harding CV. Mycobacterium tuberculosis LprA is a lipoprotein agonist of TLR2 that regulates innate immunity and APC function. *J Immunol*. 2006;177(1):422–429.
13. Gehring AJ, Dobos KM, Belisle JT, Harding CV, Boom WH. Mycobacterium tuberculosis LprG (Rv1411c): a novel TLR-2 ligand that inhibits human macrophage class II MHC antigen processing. *J Immunol*. 2004;173(4):2660–2668.
14. Gilleron M, Ronet C, Mempel M, Monsarrat B, Gachelin G, Puzo G. Acylation state of the phosphatidylinositol mannosides from Mycobacterium bovis bacillus Calmette Guerin and ability to induce granuloma and recruit natural killer T cells. *J Biol Chem*. 2001;276(37):34896–34904.
15. Means TK, Wang S, Lien E, Yoshimura A, Golenbock DT, Fenton MJ. Human toll-like receptors mediate cellular activation by Mycobacterium tuberculosis. *J Immunol*. 1999;163(7):3920–3927.
16. Beatty WL, Rhoades ER, Ullrich HJ, Chatterjee D, Heuser JE, Russell DG. Trafficking and release of mycobacterial lipids from infected macrophages. *Traffic*. 2000;1(3):235–247.
17. Bauman SJ, Kuehn MJ. Purification of outer membrane vesicles from Pseudomonas aeruginosa and their activation of an IL-8 response. *Microbes Infect*. 2006;8(9–10):2400–2408.
18. McBroom AJ, Kuehn MJ. Release of outer membrane vesicles by Gram-negative bacteria is a novel envelope stress response. *Mol Microbiol*. 2007;63(2):545–558.
19. Kremer L, et al. Identification and structural characterization of an unusual mycobacterial monomeromycolyl-diacylglycerol. *Mol Microbiol*. 2005; 57(4):1113–1126.
20. Rezwan M, Grau T, Tschumi A, Sander P. Lipoprotein synthesis in mycobacteria. *Microbiology*. 2007;153(pt 3):652–658.
21. Fahey TJ 3rd, et al. Macrophage inflammatory protein 1 modulates macrophage function. *J Immunol*. 1992;148(9):2764–2769.
22. Bansal K, Kapoor N, Narayana Y, Puzo G, Gilleron M, Balaji KN. PIM2 Induced COX-2 and MMP-9 expression in macrophages requires PI3K and Notch1 signaling. *PLoS One*. 2009;4(3):e4911.
23. Giri PK, Schorey JS. Exosomes derived from M. Bovis BCG infected macrophages activate antigen-specific CD4+ and CD8+ T cells in vitro and in vivo. *PLoS One*. 2008;3(6):e2461.
24. Besra GS, Morehouse CB, Rittner CM, Waechter CJ, Brennan PJ. Biosynthesis of mycobacterial lipoarabinomannan. *J Biol Chem*. 1997;272(29):18460–18466.
25. Schlesinger LS, Hull SR, Kaufman TM. Binding of the terminal mannosyl units of lipoarabinomannan from a virulent strain of Mycobacterium tuberculosis to human macrophages. *J Immunol*. 1994;152(8):4070–4079.
26. Nigou J, Zelle-Rieser C, Gilleron M, Thurnher M, Puzo G. Mannosylated lipoarabinomannans inhibit IL-12 production by human dendritic cells: evidence for a negative signal delivered through the mannose receptor. *J Immunol*. 2001;166(12):7477–7485.
27. Fratti RA, Backer JM, Gruenberg J, Corvera S, Deretic V. Role of phosphatidylinositol 3-kinase and Rab5 effectors in phagosomal biogenesis and mycobacterial phagosome maturation arrest. *J Cell Biol*. 2001;154(3):631–644.
28. Vergne I, Chua J, Deretic V. Tuberculosis toxin blocking phagosome maturation inhibits a novel Ca2+/calmodulin-PI3K hVPS34 cascade. *J Exp Med*. 2003;198(4):653–659.
29. Dao DN, et al. Mycobacterium tuberculosis lipomannan induces apoptosis and interleukin-12 production in macrophages. *Infect Immun*. 2004; 72(4):2067–2074.
30. Guidry TV, Hunter RL Jr, Actor JK. Mycobacterial glycolipid trehalose 6,6'-dimycolate-induced hypersensitive granulomas: contribution of CD4+ lymphocytes. *Microbiology*. 2007;153(pt 10):3360–3369.
31. Rhoades ER, Geisel RE, Butcher BA, McDonough S, Russell DG. Cell wall lipids from Mycobacterium bovis BCG are inflammatory when inoculated within a gel matrix: characterization of a new model of the granulomatous response to mycobacterial components. *Tuberculosis (Edinb)*. 2005;85(3):159–176.
32. Chen M, et al. Lipid mediators in innate immunity against tuberculosis: opposing roles of PGE2 and LXA4 in the induction of macrophage death. *J Exp Med*. 2008;205(12):2791–2801.
33. Taylor JL, et al. Role for matrix metalloproteinase 9 in granuloma formation during pulmonary Mycobacterium tuberculosis infection. *Infect Immun*. 2006;74(11):6135–6144.
34. Volkman HE, Pozos TC, Zheng J, Davis JM, Rawls JF, Ramakrishnan L. Tuberculous granuloma induction via interaction of a bacterial secreted protein with host epithelium. *Science*. 2010;327(5964):466–469.
35. Abel B, et al. Toll-like receptor 4 expression is required to control chronic Mycobacterium tuberculosis infection in mice. *J Immunol*. 2002; 169(6):3155–3162.
36. Bafica A, Scanga CA, Feng CG, Leifer C, Cheever A, Sher A. TLR9 regulates Th1 responses and cooperates with TLR2 in mediating optimal resistance to Mycobacterium tuberculosis. *J Exp Med*. 2005;202(12):1715–1724.
37. Sugawara I, Yamada H, Li C, Mizuno S, Takeuchi O, Akira S. Mycobacterial infection in TLR2 and TLR6 knockout mice. *Microbiol Immunol*. 2003; 47(5):327–336.
38. Mayer-Barber KD, et al. Caspase-1 independent IL-1beta production is critical for host resistance to mycobacterium tuberculosis and does not require TLR signaling in vivo. *J Immunol*. 2010;184(7):3326–3330.
39. Chensue SW, Warmington K, Ruth J, Lincoln P, Kuo MC, Kunkel SL. Cytokine responses during mycobacterial and schistosomal antigen-induced pulmonary granuloma formation. Production of Th1 and Th2 cytokines and relative contribution of tumor necrosis factor. *Am J Pathol*. 1994;145(5):1105–1113.
40. Chensue SW, Warmington KS, Ruth JH, Lincoln P, Kunkel SL. Cytokine function during mycobacterial and schistosomal antigen-induced pulmonary granuloma formation. Local and regional participation of IFN-gamma, IL-10, and TNF. *J Immunol*. 1995;154(11):5969–5976.
41. Gordon S. Alternative activation of macrophages. *Nat Rev Immunol*. 2003;3(1):23–35.
42. Lyadova IV, et al. In mice, tuberculosis progression is associated with intensive inflammatory response and the accumulation of gr-1 cells in the lungs. *PLoS One*. 2010;5(5):e10469.
43. Antonelli LR, et al. Intranasal Poly-IC treatment exacerbates tuberculosis in mice through the pulmonary recruitment of a pathogen-permissive monocyte/macrophage population. *J Clin Invest*. 2010;120(5):1674–1682.
44. Gabrilovich DI, Nagaraj S. Myeloid-derived suppressor cells as regulators of the immune system. *Nat Rev Immunol*. 2009;9(3):162–174.
45. Harding CV, Boom WH. Regulation of antigen presentation by Mycobacterium tuberculosis: a role for Toll-like receptors. *Nat Rev Microbiol*. 2010;8(4):296–307.
46. Schwebach JR, et al. Glucan is a component of the Mycobacterium tuberculosis surface that is expressed in vitro and in vivo. *Infect Immun*. 2002;70(5):2566–2575.
47. Besra GS. Preparation of cell-wall fractions from mycobacteria. *Methods Mol Biol*. 1998;101:91–107.
48. Laval F, Laneelle MA, Deon C, Monsarrat B, Daffe M. Accurate molecular mass determination of mycolic acids by MALDI-TOF mass spectrometry. *Anal Chem*. 2001;73(18):4537–4544.
49. Takeuchi O, et al. Differential roles of TLR2 and TLR4 in recognition of gram-negative and gram-positive bacterial cell wall components. *Immunity*. 1999;11(4):443–451.
50. Roberts AD, Belisle JT, Turner J, Gonzalez-Juarrero M, Cooper AM, Orme IM. Murine models of tuberculosis. In: Kaufmann SHE, Kabelitz D, eds. *Methods in Microbiology*. Vol. 32. Burlington, Massachusetts, USA: Academic Press Ltd; 2002:433–462.